NeuroImage 103 (2014) 163–170

Contents lists available at ScienceDirect

NeuroImage

journal homepage: www.elsevier.com/locate/ynimg

Differential functional benefits of ultra highfield MR systems within the language network

A. Geißler [a,b,c], E. Matt [a,b,c], F. Fischmeister [a,b,c], M. Wurnig [a,b,c], B. Dymerska [b,d], E. Knosp [e], M. Feucht [f], S. Trattnig [b,d], E. Auff [c], W.T. Fitch [g], S. Robinson [b,d], R. Beisteiner [a,b,c,*]

[a] Study Group Clinical fMRI, Department of Neurology, Medical University of Vienna, Austria
[b] High Field MR Center, Medical University of Vienna, Austria
[c] Department of Neurology, Medical University of Vienna, Austria
[d] Department of Biomedical Imaging and Image-guided Therapy, Medical University of Vienna, Vienna, Austria
[e] Department of Neurosurgery, Medical University of Vienna, Austria
[f] Department of Pediatrics, Medical University of Vienna, Austria
[g] Department of Cognitive Biology, University of Vienna, Vienna, Austria

ARTICLE INFO

Article history:
Accepted 15 September 2014
Available online 22 September 2014

ABSTRACT

Several investigations have shown limitations of fMRI reliability with the current standard field strengths. Improvement is expected from ultra highfield systems but studies on possible benefits for cognitive networks are lacking. Here we provide an initial investigation on a prominent and clinically highly-relevant cognitive function: language processing in individual brains. 26 patients evaluated for presurgical language localization were investigated with a standardized overt language fMRI paradigm on both 3 T and 7 T MR scanners. During data acquisition and analysis we made particular efforts to minimize effects not related to static magnetic field strength differences. Six measures relevant for functional activation showed a large dissociation between essential language network nodes: although in Wernicke's area 5/6 measures indicated a benefit of ultra highfield, in Broca's area no comparison was significant. The most important reason for this discrepancy was identified as being an increase in susceptibility-related artifacts in inferior frontal brain areas at ultra high field. We conclude that functional UHF benefits are evident, however these depend crucially on the brain region investigated and the ability to control local artifacts.

Introduction

Several recent investigations have shown limitations of fMRI reliability with the current standard field strengths (1.5–3 T, e.g. Wurnig et al., 2013). This may be problematic for conclusions drawn from neuroscientific studies or patient examinations. Limitations are due to methodological challenges which affect the functional signal change and contrast to noise ratio. Low contrast to noise is a particular problem for cognitive tasks. For example, task specific signal modulations with sophisticated language tasks may be small and signal variability typically rather large, generating a challenging situation for cognitive fMRI research. Further, contrast to noise quality is particularly critical within a clinical context. Here the challenge is to generate reliable data in single subjects without being able to average over a group, and the fMRI methods need to work with atypical morphology and functionality.

All these issues require improvement of the functional signal strength. One of the most promising approaches is to perform fMRI at ultra-high field strength (7 T) to take advantage of the considerable increase of the signal to noise ratio (SNR). In the recent history of changes in MR technology, the demonstration of increased SNR and increased BOLD sensitivity drove the historic change from 1.5 T to 3 T as the current quasi-standard technology (Speck and Turner, 2013). Correspondingly, great hopes for an improved fMRI reliability rest on 7 T ultra highfield (UHF) systems, with about 70 installations currently worldwide. However, detailed theoretical predictions regarding UHF benefits are difficult, since several factors could offset possible advances (e.g. increased artifact level, scaling of physiological noise with field strength, dependence of effects on the voxel size). Therefore experimental investigations of how much and under which task conditions SNR and contrast-to-noise (CNR) improvements occur are clearly needed, but only limited data currently exist.

A few previous fMRI studies compared 7 T with lower field strengths on healthy brains using robust sensory or motor stimulations (e.g. Geissler et al., 2013; Hahn et al., 2013; Koush et al., 2013; Triantafyllou et al., 2005; Van der Zwaag et al., 2009; Hoffmann et al.,

* Corresponding author at: Universitätsklinik für Neurologie, Währinger Gürtel 18-20, 1090 Vienna, Austria. Fax: +43 1 40400 62150.
E-mail address: roland.beisteiner@meduniwien.ac.at (R. Beisteiner).

http://dx.doi.org/10.1016/j.neuroimage.2014.09.036

2009). One previous study investigated UHF benefits in patients, also applying a motor task (tumor patients, Beisteiner et al., 2011). Concerning cognitive fMRI research, only 2 3 T–7 T studies in healthy subjects exist which investigated focal activation changes (hippocampus: Theysohn et al., 2013, amygdala: Sladky et al., 2013). There have been no studies on the benefit of UHF for the study of cognitive networks. The same holds true for cognition studies in pathological brains. Since the most prominent and also clinically most important cognitive human function is language processing, we performed the current study investigating possible functional benefits of UHF MR for investigation of the language network. The most difficult conditions for UHF are pathological brains, which represent the worst case scenario for signal variability and methodological challenges. If an increased sensitivity for cognitive networks can be demonstrated here, UHF benefits are even more likely for healthy brains. For that reason we acquired data of tumor patients and – as in our previous study with a motor task — functional signal was assessed in non-transformed (non-normalized) individual brains. This is important to be able to extend conclusions about possible cognitive network benefits to the clinical environment where UHF benefits are required for individuals rather than groups.

Materials and methods

Patients

The study was approved by the local ethics committee of the Medical University of Vienna. All patients participated with written informed consent. To allow a realistic evaluation of UHF benefits for typical clinical populations all patients who were referred for presurgical language localization in a given period were considered for inclusion in this study. The requests for presurgical planning were not influenced by the authors and therefore included 3 patients with only right hemispheric pathology (see Table 1 for demographic and clinical details). Other than the receipt of an external request for language localization, the only inclusion criterion was the ability to perform the task and tolerate two fMRI measurement sessions. Exclusion criteria were clinical or MR contraindications. At the time of measurement, all twenty six right-handed patients (10 females, mean age 26.8 years old and 16 males, mean age 35.71 years old; age range 8–69 years of age) were in good general health and could perform the task well. Clinical fMRI reports were generated with a different analysis from that presented in this study, and are not reported here.

Task

The language task was an overt speech paradigm (Foki et al., 2008; Gartus et al., 2009) which reproduces typical everyday communication demands. The basic experimental setup comprised 20 pseudorandomized block-designed fMRI runs of a syntactic (10 runs) and a semantic task (10 runs). Each run consisted of 4 control and 3 activation periods with duration of 20 s each. During an activation period, two 5-word sentences were automatically presented word by word. The final word consisted of 2 alternative verbs that were either syntactically or semantically correct or incorrect (cf. Gartus et al., 2009). One sentence was displayed for 10 s. The instruction was to read overtly every word and to repeat the correct final sentence. All subjects were trained to speak softly and to minimize movements of head and facial muscles. Depending on the patient's tolerance and performance, between 9 and 20 complete runs were acquired.

Image acquisition

All subjects were examined with both a Siemens 3 T whole body MAGNETOM TIM TRIO scanner and a Siemens MAGNETOM 7 T whole body scanner (Siemens Healthcare, Erlangen, Germany). A 32 channel head coil was used at 3 T (Siemens Healthcare). Due to ongoing hardware upgrades, a few patients scanned at 7 T were measured with an 8 or 24 channel head coil but most of the measurements were done with a 32 channel head coil (Nova Medical, Wilmington Massachusetts, USA). Measurements at 3 T and 7 T were carried out with an average separation of 7.21 (SD: 10.56) days and system order was randomized. To minimize head motion artifacts, individually constructed plaster cast helmets (Edward et al., 2000) were used on both systems. On both systems functional data were acquired with a 2D single shot gradient-echo (GE) EPI sequence, with slices aligned parallel to the AC–PC plane and whole brain coverage. As in Beisteiner et al. (2011), efforts were made

Table 1
Demographic and clinical details.

Patient	Sex	Age	Localization of pathology	Pathological diagnosis at the time of fMRI
P1	F	20	Right frontal	Low grade glioma
P2	M	67	Left parietal postcentral	Tumor of unknown origin
P3	M	34	Left fronto-temporal	Recurrent astrocytoma grade II
P4	F	14	Left temporal	Temporal lobe epilepsy
P5	M	21	Right central	Low grade glioma central
P6	F	39	Left temporo-parietal	Astrocytoma
P7	F	18	Left temporal	Temporal lobe epilepsy, hippocampus atrophy and sclerosis, previous partial resection
P8	M	12	Left temporal	Temporal lobe epilepsy
P9	F	38	Left frontal	Low grade glioma
P10	F	47	Left frontal	Recurrent glioma
P11	M	64	Left opercular	Grade II astrocytoma
P12	F	13	Left parieto-temporo-occipital	Epilepsy, focal cortical dysplasia
P13	M	69	Left temporo-parietal	Tumor of unknown origin
P14	M	38	Left frontal	Recurrent low grade glioma
P15	F	8	Bilateral frontal and occipital	Frontal lobe epilepsy, bilateral dysplasia
P16	M	27	Left temporo-parietal	Tumor of unknown origin
P17	M	38	Left temporal	Cavernoma
P18	M	37	Left fronto-temporal	Low grade glioma
P19	M	17	Left temporo-occipital	Epilepsy, tumor of unknown origin
P20	F	12	Right occipital	Epilepsy, cystic lesion
P21	M	23	Left frontal	Low grade glioma
P22	F	54	Left precentral	Tumor of unknown origin
P23	M	32	Left insular	Tumor of unknown origin
P24	M	35	Left frontal	Recurrent tumor of unknown origin
P25	F	35	Left insular	Grade II astrocytoma
P26	M	38	Left frontal	Low grade astrocytoma

to avoid confounding effects not primarily related to static magnetic field strength and – with the principal exception of echo time (TE) – keep measurement parameters consistent between systems where possible. System specific sequence adaptations were minimized (e.g. according to specific absorption rate (SAR) guidelines, whole brain coverage requirements, different TE values).

Common sequence parameters

On both systems FOV 230 mm, matrix size of 128 × 128 × 34, 56 repetitions, slice thickness 3 mm and TR 2500 ms were used. We also applied parallel imaging with GRAPPA-iPAT factor 2, fat suppression by a chemical shift selective saturation pulse prior to every slice and 10 s of dummy scans.

Differing sequence parameters

3 T: TE 28 ms, bandwidth 2220 Hz, flip angle 90°, full Fourier encoding, no gap between slices. Vendor provided fat saturation module with a preset flip angle of 110°.

7 T: TE 22 ms, bandwidth 1445 Hz, flip angle 80°, 6/8 partial Fourier factor (omitting the first 25% of k-space phase-encoding lines), 10% gap between slices. The effective echo time at 7 T was optimized via assessment of T2* for this resolution. Flip angles of the vendor-provided fat saturation module was reduced to 90° due to specific absorption rate (SAR) limitations.

Field maps

To get investigate area-specific image distortions in a subsample of patients, B0 field maps were acquired for six patients at 7 T (for 5 patients with the 24 channel coil, for one patient with the 8 channel coil). With the 24 channel coil field maps were acquired with a triple-echo (TE = 4.6, 9.3, 14.1 ms) gradient-echo (GE) sequence and with the 8 channels with a dual-echo (TE = 10.0, 13.9 ms) GE sequence. Other field map parameters were consistent for all patients: TR = 1010 ms, FA = 30° and fat saturation, 53 AC–PC axial slices of 2 mm thickness with 0.3 mm gap, 128 × 128 matrix, FOV 230 mm, pixel bandwidth = 260 Hz and GRAPPA factor 2 in the same geometry as the GE-EPIs.

Structural image

High-resolution T1-weighted MR images were acquired using a 3D MPRAGE sequence with a matrix size of 320 × 320 × 224, with 0.7 mm isotropic resolution, flip angle of 9° and GRAPPA acceleration factor 2; acquisition time 7 min and 57 s.

fMRI data analysis

With every patient the same number of artifact free 3 T and 7 T runs was entered into the analysis. All superfluous runs were excluded (by acquisition order, to avoid bias). Functional data were pre-processed and statistical analysis was performed using SPM8 (Wellcome Department of Imaging Neuroscience, London, UK; http://www.fil.ion.ucl.ac.uk/spm). To reduce residual small-scale motion, all runs were registered to the first scan using default settings, except that the factors "Quality: 0.95" and "Separation: 2" were used to improve correction quality. No slice timing correction or spatial normalization was carried out. Functional images were smoothed with a 4 × 4 × 6 mm full width at half maximum (FWHM) Gaussian kernel. First level statistical analysis was performed with a fixed effects analysis (SPM default settings, no additional temporal filtering or averaging) with inclusion of motion parameters in the design matrix as nuisance variables. BOLD responses were modeled by a fixed response boxcar function convolved with the canonical hemodynamic response. Activation was established for each patient via voxel-wise t-tests to generate individual SPM t-maps.

Definition of the particular target areas (Broca's and Wernicke's areas)

To allow inferences about benefits for individual subjects and minimize postprocessing related confounds (Beisteiner et al., 2010) all functional analyses were performed on non-transformed (non-normalized) individual data (Fig. 1). The analysis was focused on left hemispheric essential areas of the language network (Broca's and Wernicke's areas) as the most relevant with regard to a possible functional signal improvement. In addition, these areas provide an important dichotomy concerning their susceptibility to artifacts: Wernicke lies in the posterior superior temporal gyrus, a relatively magnetically homogeneous region while Broca, in the inferior frontal cortex, is subject to much higher susceptibility-related field gradients. Broca and Wernicke activation clusters were defined for every patient by a clinical fMRI expert (RB) on the basis of the individual SPM t-maps and the existing functional medical reports. This was done for both field strengths. Afterwards the voxels with the highest t-values in each Broca and Wernicke cluster were identified. These peak voxels served as the center for patient-specific spherical regions of interest (ROI), which had a radius of 5 mm. To avoid the inclusion of non-brain areas (e.g. scalp, skull) ROIs were defined on the skull-stripped mean EPI volume (BET2 with a subject specific fractional intensity threshold, Jenkinson et al., 2002). Spherical ROIs were cropped at the brain border if necessary. Further analysis was limited to these ROIs.

Quantification of functional activation

Quantification was based on the individual suprathreshold ROI voxels as separately defined for the 3 T and 7 T experiments (whole brain analysis, $p <= 0.05$, FWE corrected). To assess effects related to the two field strengths, we compared six measures relevant to functional activation (Beisteiner et al., 2011): (1) voxel count (number of suprathreshold voxels), (2) mean t-value, (3) peak SPM t-value, (4) percentage signal change, (5) contrast to noise ratio (CNR) (Geissler et al., 2007) and (6) peak CNR.

Measures: (1) voxel count, (2) mean t-value and (3) peak t-value. For each patient, all voxels included in the ROI were analyzed for the 3 T and 7 T experiments separately. The voxel count (the number of voxels in the ROI), the mean t-value of all ROI voxels and the highest t-value of all ROI voxels were determined.

Measure (4): percentage signal change. Percentage signal change, ΔS/SOFF, was calculated according to the definition of Van der Zwaag et al. (2009). In brief, ΔS = (SON − SOFF), where SON is the mean absolute signal of all time points within "ON" phases and SOFF is the mean of all time points within "OFF" phases (arithmetic mean, voxel-wise calculation). For the definition of ON and OFF phases the underlying block design of the paradigm was shifted by 5 s to accord with the delayed BOLD response. This calculation was performed for all voxels within the ROI separately for every run of each patient followed by arithmetic averaging to achieve one representative value per patient and field strength.

Measures: (5) contrast to noise ratio (CNR) and (6) peak contrast to noise ratio. CNR was calculated from ΔSCNR/σt-noise, as defined in Geissler et al. (2007). Essentially, the contrast ΔSCNR is the averaged voxel-wise signal change in the temporally smoothed original signal: (mean value of all time points within the "ON" phase) − (mean value of all time points within the "OFF" phase). ON/OFF definitions were the same as for the percentage signal change analysis (measure 4, see above). Smoothing was performed using a Savitzky–Golay filter with a polynomial order of 2 and length 5. σt-noise is the non-task-related variability over time — in this case the standard deviation of the difference between the original and smoothed signals. Again, this calculation was performed for all voxels within the ROI and every run of each patient, followed by arithmetic averaging to achieve one representative value per patient and field strength. The peak CNR for each patient and field strength was determined by analyzing the mean CNR values of all ROI voxels separately for the 3 T and 7 T experiments.

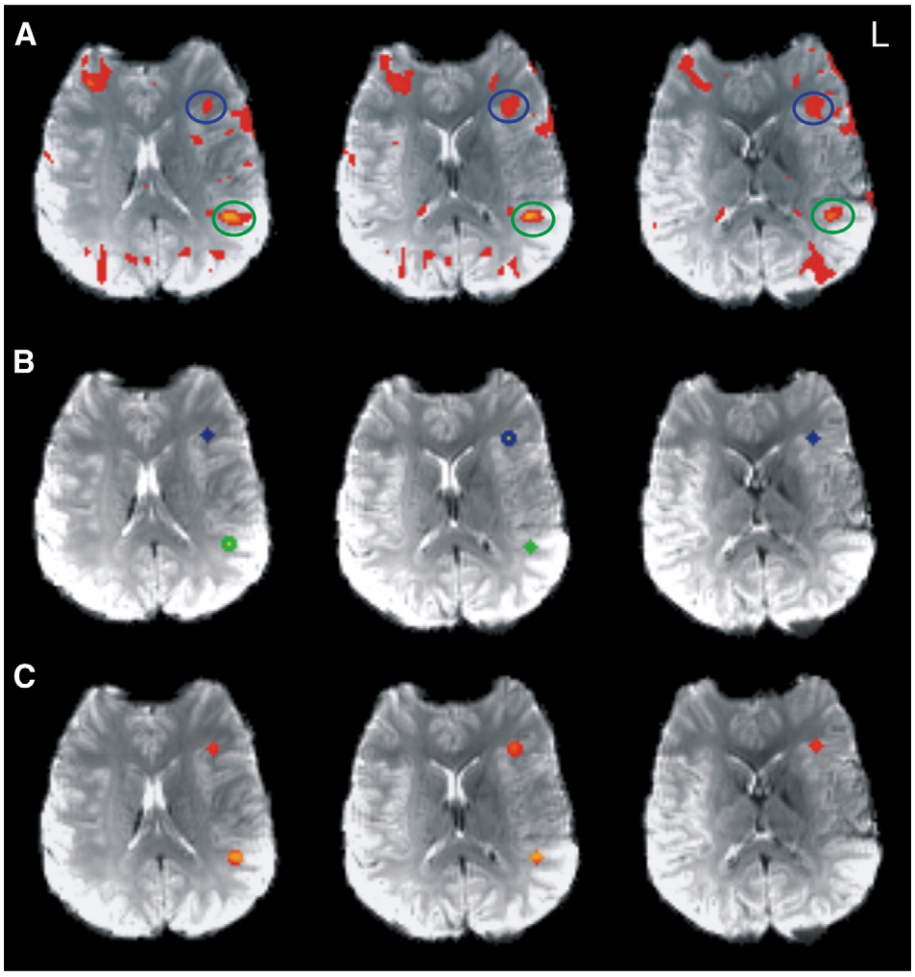

Fig. 1. ROI generation in a representative patient (P 16) at 7 T. A: SPM-t-map ($p < 0.05$, FWE corrected) with Broca (blue circle) and Wernicke activations (green circle). B: Peak voxel (yellow) served as the center for a patient specific spherical region of interest (ROI) with a radius of 5 mm for Broca's area (blue) and Wernicke's area (green). C: Suprathreshold voxels within the ROIs.

Quantification of image quality

Since patient motion leads to ghost-like artifacts in accelerated acquisitions (Skare et al., 2007) and parallel imaging was used at both field strengths (GRAPPA factor 2 (Griswold et al., 2002)), we evaluated 2 measures of image quality. The absolute ghost to signal ratio (GSR_A) was calculated, and magnetic field gradients in Broca's and Wernicke's areas were assessed in a subgroup of patients. Ghost to signal ratio (GSR_A) was calculated similar to the approach used in the EU COMAC-BME II project (Lerski and de Certaines, 1993). This measure is defined as the relation of the mean ghosting signal S_{ghost} within 2 ghost contained ROIs and the mean signal within a homogenous white matter ROI S_{WM}. ROI selection for this purpose was performed on the 3 central slices of the functional EPI dataset. The white matter ROI S_{WM} was located in a central undisturbed white matter area. The 2 ghost ROIs were located anterior and posterior of the brain and comprised possible ghosting artifacts in the phase-encode direction (Fig. 2).

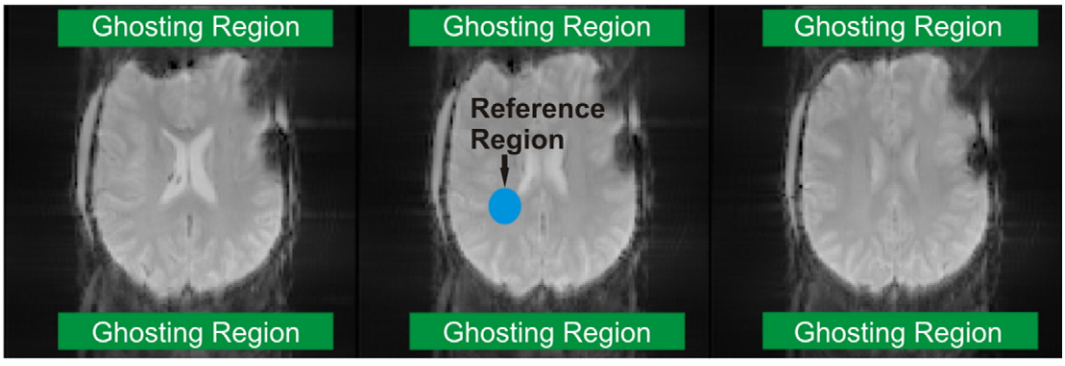

Fig. 2. EPI images for visualizing of ghosting artifacts (P7, 7 T data). Green: ROIs for detection of ghosting signals, blue: central reference ROI. The relation between the mean absolute signals within the ghosting ROIs and the reference ROIs was calculated.

Table 2
Summary of the 3 T and 7 T results.

Measure	3 T value (SD)	7 T value (SD)	p-Value
Broca			
Voxel count	27.6 (13.3)	24.8 (15.5)	n.s.
Mean t-value	7.2 (1.3)	7.7 (2.7)	n.s.
Peak t-value	9.4 (2.5)	10.2 (3.8)	n.s.
Percentage signal change (%, mean of fROI)	1.0 (0.8)	1.6 (1.7)	n.s.
Contrast to noise ratio (CNR)	1.5 (0.7)	1.6 (0.7)	n.s.
Peak CNR	2.2 (0.9)	2.2 (1.1)	n.s.
Wernicke			
Voxel count	30.2 (14.7)	32.6 (15.0)	n.s.
Mean t-value	8.3 (2.7)	11.1 (4.4)	0.004
Peak t-value	11.5 (4.7)	16.3 (6.6)	0.0007
Percentage signal change (%, mean of fROI)	1.1 (0.5)	1.5 (0.7)	0.005
Contrast to noise ratio (CNR)	1.9 (0.7)	2.3 (0.9)	0.006
Peak CNR	2.8 (1.3)	3.9 (1.7)	0.0002
Motion indication			
Translation (mm)	0.09 (0.05)	0.17 (0.08)	0.00004
Rotation (rad)			
Pitch	8.9E−4 (9.1E−4)	1.1E−3 (7.0E−4)	n.s.
Roll	3.7E−4 (1.7E−4)	5.3E−4 (3.1E−4)	0.004
Yaw	2.9E−4 (1.3E−4)	4.0E−4 (2.6E−4)	0.017
Static image quality			
GSR_A	5.3E−2 (1.2E−2)	1.1E−1 (6.9E−2)	0.00013

Using the SPM motion parameters, we also calculated group mean translational and rotational (pitch, roll, yaw) head motion during 3 T and 7 T experiments.

To explore possible differences in image distortions (and potential signal loss) between Broca's and Wernicke's areas, in a sample of six patients field maps were generated from additional multi-echo gradient echo (MGE) measurements performed at 7 T. This was done as described in Robinson and Jovicich (2011) using a freely available MATLAB toolbox (http://www.mathworks.com/matlabcentral/fileexchange/30853-field-mapping-toolbox). The Hermitian inner product was used to generate phase difference images. The gradient of field maps in the primary imaging axes was calculated using MATLAB and the length of the gradient vector G_{length} [rad·Hz / voxel] was calculated using the Euclidean norm. Finally, the mean length inside each enlarged (R = 10 mm) version of the spherical Wernicke and Broca regions of interest was determined (Table 3).

Statistical evaluation of 3 T–7 T differences

After testing for normally distributed data, paired t-tests comparing 3 T and 7 T values were calculated over all patients for voxel count, mean t-value, peak t-value, percentage signal change, CNR, peak CNR and SNR.

Results

The clinical reports demonstrated left hemispheric Broca and Wernicke activations with all patients and mostly a left hemispheric dominance. The clinical reports had been generated from the same

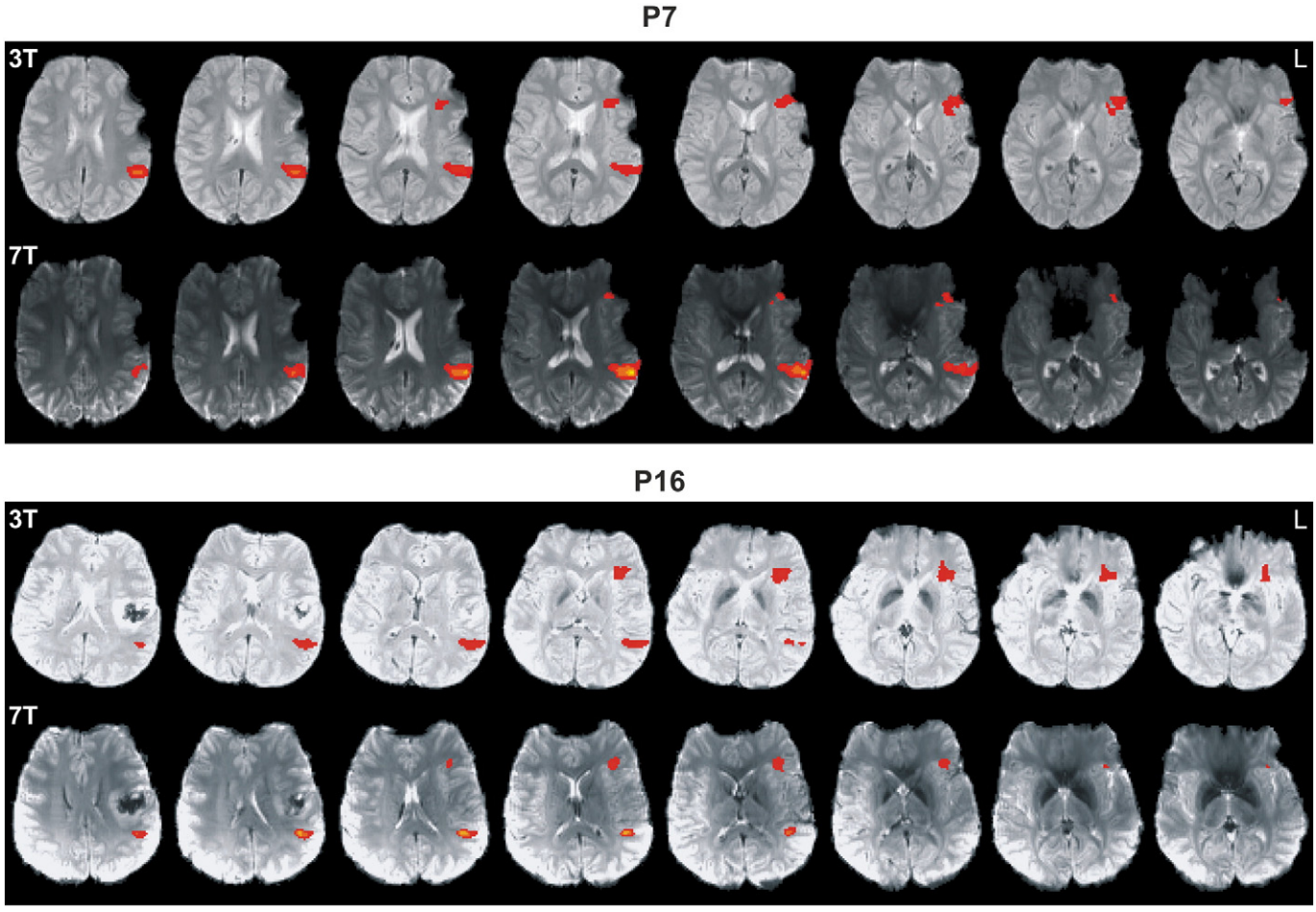

Fig. 3. Functional MRI data (FWE < 0.05, left hemisphere on the right) of P7 and P16 comparing corresponding 3 T and 7 T functional activations. Note extended postoperative artifacts with P7. In contrast to the 7 T benefit for Wernicke's area, there is a clear 7 T signal loss in Broca's area.

data, however using the local risk map technique which includes an evaluation of the reliability of activations achieved with repetitive runs and based on different reference functions (Beisteiner et al., 2000, 2010). Statistical results of the ROI analysis of the present study are summarized in Table 2 and Figs. 3, 4. Due to investigating non-normalized data, no MNI coordinates for slices/brain activations can be given.

Quantification of functional activation

Within Wernicke's area, 5 of 6 measures showed a significant improvement of functional sensitivity for the 7 T measurements. In Broca's area, in contrast, no measure demonstrated a significant benefit for the 7 T system. In detail, the measures (2) mean t-value, (3) peak t-value, (4) percentage signal change, (5) contrast to noise ratio and (6) peak contrast to noise ratio show significant 7 T benefits in Wernicke's

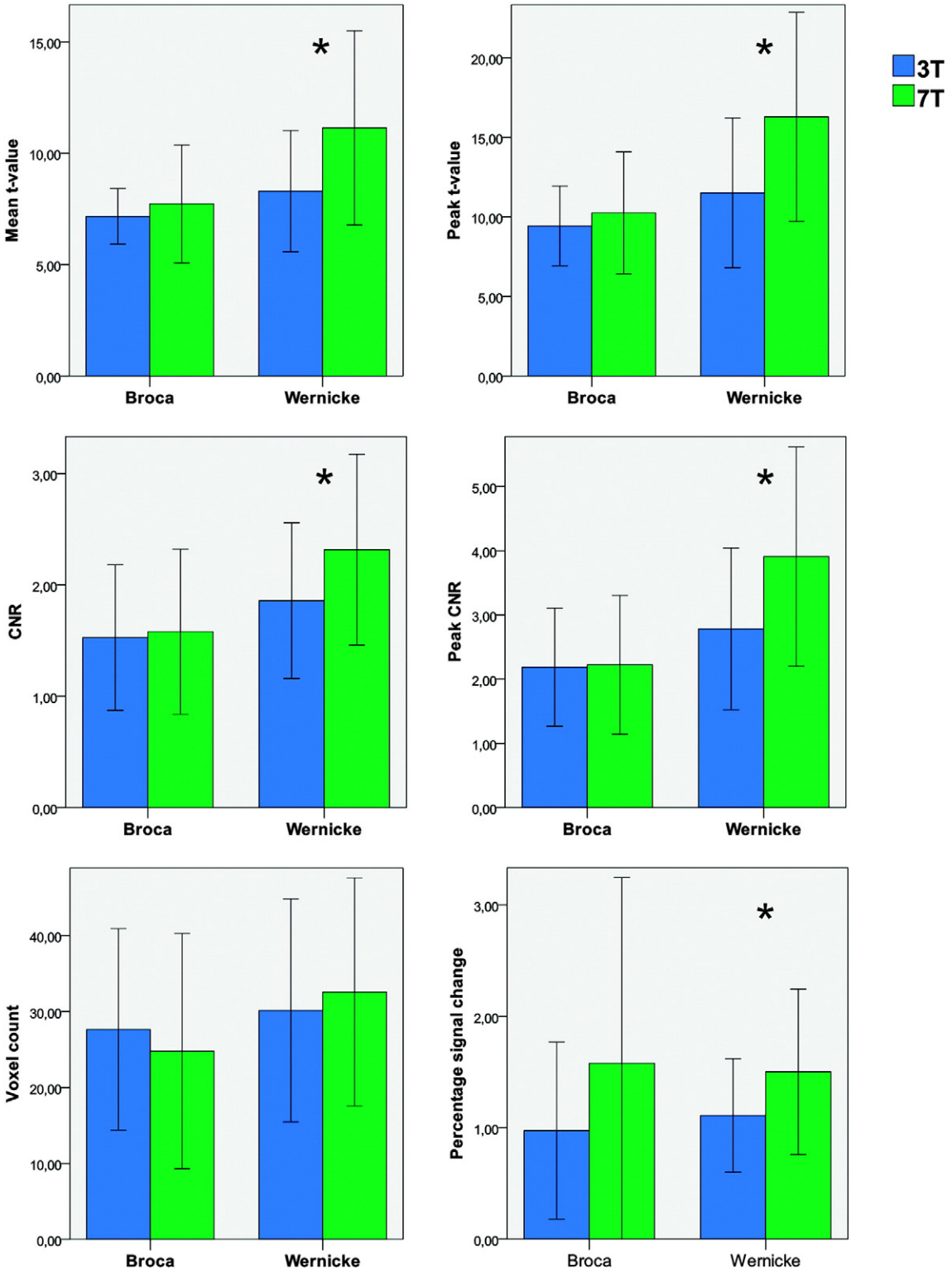

Fig. 4. Broca/Wernicke behavior of the functional activation measures (compare Table 2). Only Wernicke's area showed a significant (marked by an asterisk "*") ultra highfield benefit. Error bars indicate standard deviation.

area. Measure (1) voxel count did not show a 7 T benefit, neither for Wernicke's area nor for Broca's area (Table 2).

Quantification of image quality

Analysis of ghosting artifacts showed a significantly increased GSR_A level in 7 T, particular in Nyquist ghosting and parallel imaging reconstruction errors (Table 2). This means that ghosting artifacts are larger with 7 T measurements. Head motion, which also worsens parallel imaging reconstruction errors, was also significantly larger for the 7 T measurements (except pitch direction, Table 2). Evaluation of 7 T image distortions in Broca's and Wernicke's areas showed that the mean magnetic field gradient in Broca's area was higher than that in Wernicke's area for all patients, and this difference was statistically significant (Wilcoxon Signed Ranks Test, Table 3). This indicates that missing functional signal benefits for 7 T in Broca's area are most likely due to larger magnetic field inhomogeneities there.

Discussion

This study provides the first data quantifying possible UHF fMRI benefits for the investigation of cognitive networks. As a prominent and clinically-relevant cognitive function, we selected the language network for this investigation. The results show that different network components may benefit differently from UHF systems, despite representing the same level of functional significance (Broca's and Wernicke's areas both represent essential language cortex). We made significant efforts to minimize all effects not related to B0 field strength differences by two approaches. First, variations in experimental parameters (including voxel size) and MR hardware (manufacturers, coil types) were kept as minimal as possible. Second, possible effects of post-processing – which may influence fMRI results, particularly for pathological brains – were minimized: all signal parameters were calculated from original (non-transformed) functional EPI images using identical methodology for 3 T and 7 T.

The dissociation of UHF benefits within the language network was considerable in our population (Broca 0/6–Wernicke 5/6 parameters significant). This indicates that a functional UHF benefit is readily achievable for superior temporal and central areas (motor system, Beisteiner et al., 2011), however improvements were not evident for inferior frontal areas. The most likely explanation for this is the increased susceptibility-related field gradients in inferior frontal brain areas causing increased artifacts at UHF. This is evidenced by the original functional EPI images (Fig. 3) and the field map results. Field maps show significantly larger gradients in B0 in Broca's compared to Wernicke's area, causing increased signal dropouts. As gradients in B0 scale approximately linearly with field strength, signal loss in Broca's area is considerably lower with our 3 T data. As with our previous study, ghosting and head motion artifacts were also larger at 7 T compared to 3 T, although these should not differentially affect Broca's and Wernicke's areas. The same is true for possible environmental factors like psychological effects due to varying comfort (the 3 T system has a shorter bore, and is more brightly lit). Such environmental factors are unlikely to confound signal changes such that UHF sensitivity is only reduced for Broca's area.

Concerning limitations of the study, it is important to realize that secure conclusions can only be drawn for the particular population and the specific cognitive network studied. Our population represents a typical one for cognitive clinical fMRI applications with varying locations and extensions of pathologies, only partially and not systematically affecting Broca and Wernicke cortexes. It cannot be excluded that our results are influenced by these pathologies (e.g. tumor vessels and inhomogeneities can lead to false positive results), and would be different with healthy populations. On the other hand, the general anatomical conditions for frontal and superior temporal brain areas are also present in healthy brains (particularly the brain–air relationship in inferior frontal cortex). Inferior frontal regions are generally more prone to susceptibility-related signal loss than superior temporal brain areas — and the problem of signal loss scales with field strength. A casual subanalysis which we performed on a patient subset lacking an inferior frontal pathology supports this view since it showed the same functional sensitivity lack for Broca's compared to Wernicke's area.

Another issue relevant for generalizing conclusions from our current data concerns the possibility that extended 7 T specific optimizations of the experimental setup and the MR sequences might increase the chances to generate a functional UHF benefit for Broca's area as well. Such procedures could counteract the known increase of imaging problems at very high field (e.g. geometric distortions (Robinson and Jovicich, 2011), signal dropouts and an increase in parallel imaging artifacts (Beisteiner et al., 2011; Skare et al., 2007)). For example, 3D-EPI acquisition techniques (Poser et al., 2010; Van der Zwaag et al., 2012) provide a better image quality and less artifacts in critical brain regions at 7 T. The field strength dependent increase of BOLD noise at 7 T compared to 3 T can be reduced by a reduction of slice thickness and voxel size at 7 T, leading to artifact reduction in critical brain regions and nevertheless a sufficient signal gain (Triantafyllou et al., 2011). However, we did not choose this approach since it would inevitably increase the methodological differences between the 3 T and 7 T experiments which we attempted to minimize. For this initial cognitive network investigation studying potential UHF benefits, we wanted to apply a field strength comparison with widely used and clinically implemented standard technologies. This should be most practically relevant and informative with respect to pure field strength effects, however does not allow conclusions about maximum 7 T benefits achievable under specific experimental conditions. Note, that smaller voxel sizes are typically not necessary for the evaluation of cognitive network activations and would bias a pure field strength comparison against 3 T. Overall, our approach allows inferences as to where UHF benefits may be expected without special application conditions (such as custom hardware, non-standard sequences, or preselected participants).

In summary, our data indicate that the functional UHF benefits reported by most prior UHF studies do not immediately and unambiguously translate to cognitive networks. For a comprehensive picture and particularly for clinical applications it will be important to extend the current database about the network types and network nodes for which UHF gains occur. This will require future studies on other cognitive networks and also on the ameliorating effects of technical improvements. Promising candidates for improvement include system specific sequence optimizations, multiband imaging (Setsompop et al., 2012), dynamic distortion correction techniques (Xiang and Ye, 2007) and sequences which are less prone to reconstruction errors in the presence of motion and are inherently virtually free of Nyquist ghosting (Poser et al., 2013). From the present data our conclusion is that functional UHF benefits are evident, however these depend crucially on the brain region investigated and the ability to control local artifacts.

Table 3
Field map results.

Patient	G_{length} [rad·Hz / voxel]		Difference [rad·Hz / voxel]
	Broca's area	Wernicke's area	Broca–Wernicke
P1	61.458	28.087	33.371
P5	123.951	71.466	52.485
P13	128.792	64.285	64.507
P17	30.892	8.854	22.038
P20	59.176	30.096	29.08
P22	82.068	28.638	53.43
Statistical tests			
Wilcoxon	0.028		
Sign Test	0.031		

Acknowledgment

This study was supported by the Vienna Spots of Excellence Program of the Centre of Innovation and Technology, City of Vienna (ZIT), University grant number FA102A001, a research cluster grant "Shared Neural Resources for Music and Language" to WTF and RB (University of Vienna and Medical University of Vienna) and the Austrian Science Fund (FWF) project KLI264.

References

Beisteiner, R., Lanzenberger, R., Novak, K., Edward, V., Windischberger, C., Erdler, M., Cunnington, R., Gartus, A., Streibl, B., Moser, E., Czech, Th., Deecke, L., 2000. Improvement of presurgical evaluation by generation of FMRI risk maps. Neurosci. Lett. 290, 13–16.

Beisteiner, R., Klinger, N., Höllinger, I., Rath, J., Gruber, S., Steinkellner, T., Foki, T., Geissler, A., 2010. How much are clinical fMRI reports influenced by standard postprocessing methods? An investigation of normalization and region of interest effects in the medial temporal lobe. Hum. Brain Mapp. 31 (12), 1951–1966. http://dx.doi.org/10.1002/hbm.20990 (Dec).

Beisteiner, R., Robinson, S., Wurnig, M., Hilbert, M., Merksa, K., Rath, J., Höllinger, I., Klinger, N., Ch, Marosi, Trattnig, S., Geissler, A., 2011. Clinical fMRI: evidence for a 7 T benefit over 3 T. Neuroimage 57 (3), 1015–1021. http://dx.doi.org/10.1016/j.neuroimage.2011.05.010 (Aug 1).

Edward, V., Windischberger, C., Cunnington, R., Erdler, M., Lanzenberger, R., Mayer, D., Endl, W., Beisteiner, R., 2000. Quantification of fMRI artifact reduction by a novel plaster cast head holder. Hum. Brain Mapp. 11 (3), 207–213 (Nov).

Foki, T., Gartus, A., Geissler, A., Beisteiner, R., 2008. Probing overtly spoken language at sentential level: a comprehensive high-field BOLD–fMRI protocol reflecting everyday language demands. Neuroimage 39 (4), 1613–1624 (Feb 15).

Gartus, A., Foki, T., Geissler, A., Beisteiner, R., 2009. Improvement of clinical language localization with an overt semantic and syntactic language functional MR imaging paradigm. AJNR Am. J. Neuroradiol. 30 (10), 1977–1985. http://dx.doi.org/10.3174/ajnr.A1725 (Nov).

Geissler, A., Gartus, A., Foki, T., Tahamtan, A.R., Beisteiner, R., Barth, M., 2007. Contrast-to-noise ratio (CNR) as a quality parameter in fMRI. J. Magn. Reson. Imaging 25 (6), 1263–1270 (Jun).

Geißler, A., Fischmeister, F.P., Grabner, G., Wurnig, M., Rath, J., Foki, T., Matt, E., Trattnig, S., Beisteiner, R., Robinson, S.D., 2013. Comparing the microvascular specificity of the 3- and 7-T BOLD response using ICA and susceptibility-weighted imaging. Front. Hum. Neurosci. 7, 474. http://dx.doi.org/10.3389/fnhum.2013.00474. PubMed PMID: 23950744.

Griswold, M.A., Jakob, P.M., Heidemann, R.M., Nittka, M., Jellus, V., Wang, J., Kiefer, B., Haase, A., 2002. Generalized autocalibrating partially parallel acquisitions (GRAPPA). Magn. Reson. Med. 47 (6), 1202–1210 (Jun).

Hahn, A., Kranz, G.S., Seidel, E.M., Sladky, R., Kraus, C., Küblböck, M., Pfabigan, D.M., Hummer, A., Grahl, A., Ganger, S., Windischberger, C., Lamm, C., Lanzenberger, R., 2013. Comparing neural response to painful electrical stimulation with functional MRI at 3 and 7 T. Neuroimage 12 (82C), 336–343. http://dx.doi.org/10.1016/j.neuroimage.2013.06.010 (Jun).

Hoffmann, M.B., Stadler, J., Kanowski, M., Speck, O., 2009. Retinotopic mapping of the human visual cortex at a magnetic field strength of 7 T. Clin. Neurophysiol. 120 (1), 108–116. http://dx.doi.org/10.1016/j.clinph.2008.10.153 (Jan).

Jenkinson, M., Bannister, P., Brady, M., Smith, S., 2002. Improved optimization for the robust and accurate linear registration and motion correction of brain images. Neuroimage 17 (2), 825–841 (Oct).

Koush, Y., Elliott, M.A., Scharnowski, F., Mathiak, K., 2013. Real-time automated spectral assessment of the BOLD response for neurofeedback at 3 and 7 T. J. Neurosci. Methods 218 (2), 148–160. http://dx.doi.org/10.1016/j.jneumeth.2013.05.002 (Sep 15).

Lerski, R.A., de Certaines, J.D., 1993. Performance assessment and quality control in MRI by Eurospin test objects and protocols. Magn. Reson. Imaging 11 (6), 817–833.

Poser, B.A., Koopmans, P.J., Witzel, T., Wald, L.L., Barth, M., 2010. Three dimensional echo-planar imaging at 7 Tesla. Neuroimage 51 (1), 261–266. http://dx.doi.org/10.1016/j.neuroimage.2010.01.108 (May 15).

Poser, B.A., Barth, M., Goa, P.E., Deng, W., Stenger, V.A., 2013. Single-shot echo-planar imaging with Nyquist ghost compensation: interleaved dual echo with acceleration (IDEA) echo-planar imaging (EPI). Magn. Reson. Med. 69 (1), 37–47.

Robinson, S., Jovicich, J., 2011. B0 mapping with multi-channel RF coils at high field. Magn. Reson. Med. 66 (4), 976–988. http://dx.doi.org/10.1002/mrm.22879 (Oct).

Setsompop, K., Cohen-Adad, J., Gagoski, B.A., Raij, T., Yendiki, A., Keil, B., Wedeen, V.J., Wald, L.L., 2012. Improving diffusion MRI using simultaneous multi-slice echo planar imaging. Neuroimage 63 (1), 569–580. http://dx.doi.org/10.1016/j.neuroimage.2012.06.033 (Oct 15).

Skare, S., Newbould, R.D., Clayton, D.B., Albers, G.W., Nagle, S., Bammer, R., 2007. Clinical multishot DW-EPI through parallel imaging with considerations of susceptibility, motion, and noise. Magn. Reson. Med. 57 (5), 881–890 (May).

Sladky, R., Baldinger, P., Kranz, G.S., Tröstl, J., Höflich, A., Lanzenberger, R., Moser, E., Windischberger, C., 2013. High-resolution functional MRI of the human amygdala at 7 T. Eur. J. Radiol. 82 (5), 728–733. http://dx.doi.org/10.1016/j.ejrad.2011.09.025 (May).

Speck, O., Turner, R., 2013. Neurofunctional MRI at high magnetic fields. Radiologe 53 (5), 415–421. http://dx.doi.org/10.1007/s00117-012-2345-9 (May).

Theysohn, N., Qin, S., Maderwald, S., Poser, B.A., Theysohn, J.M., Ladd, M.E., Norris, D.G., Gizewski, E.R., Fernandez, G., Tendolkar, I., 2013. Memory-related hippocampal activity can be measured robustly using FMRI at 7 Tesla. J. Neuroimaging 23 (4), 445–451. http://dx.doi.org/10.1111/jon.12036 (Oct).

Triantafyllou, C., Hoge, R.D., Krueger, G., Wiggins, C.J., Potthast, A., Wiggins, G.C., Wald, L.L., 2005. Comparison of physiological noise at 1.5 T, 3 T and 7 T and optimization of fMRI acquisition parameters. Neuroimage 26 (1), 243–250 (May 15).

Triantafyllou, C., Polimeni, J.R., Wald, L.L., 2011. Physiological noise and signal-to-noise ratio in fMRI with multi-channel array coils. Neuroimage 55 (2), 597–606. http://dx.doi.org/10.1016/j.neuroimage.2010.11.084 (Mar 15).

Van der Zwaag, W., Francis, S., Head, K., Peters, A., Gowland, P., Morris, P., Bowtell, R., 2009. fMRI at 1.5, 3 and 7 T: characterising BOLD signal changes. Neuroimage 47 (4), 1425–1434. http://dx.doi.org/10.1016/j.neuroimage.2009.05.015 (Oct 1).

Van der Zwaag, W., Marques, J.P., Kober, T., Glover, G., Gruetter, R., Krueger, G., 2012. Temporal SNR characteristics in segmented 3D-EPI at 7 T. Magn. Reson. Med. 67 (2), 344–352. http://dx.doi.org/10.1002/mrm.23007 (Feb).

Wurnig, M.C., Rath, J., Klinger, N., Höllinger, I., Geissler, A., Fischmeister, F.P., Aichhorn, M., Foki, T., Kronbichler, M., Nickel, J., Siedentopf, C., Staffen, W., Verius, M., Golaszewski, S., Koppelstätter, F., Knosp, E., Auff, E., Felber, S., Seitz, R.J., Beisteiner, R., 2013. Variability of clinical functional MR imaging results: a multicenter study. Radiology 268 (2), 521–531 (Aug).

Xiang, Q.S., Ye, F.Q., 2007. Correction for geometric distortion and N/2 ghosting in EPI by phase labeling for additional coordinate encoding (PLACE). Magn. Reson. Med. 57 (4), 731–741 (Apr).